Initial-state interactions for K^--proton radiative capture

Peter B. Siegel
California State Polytechnic University, Pomona California 91768

Bijan Saghai
Service de Physique Nucléaire, CEA/DSM/DAPNIA, Centre d'Études de Saclay, F-91191 Gif-sur-Yvette, France

(Received 22 November 1994)

The effects of the initial-state interactions on the K^--p radiative capture branching ratios are examined and found to be quite sizable. A general coupled-channel formalism for both strong and electromagnetic channels using a particle basis is presented, and applied to all the low energy K^--p data with the exception of the *1s* atomic level shift. Satisfactory fits are obtained using vertex coupling constants for the electromagnetic channels that are close to their expected SU(3) values.

PACS number(s): 13.75.Jz, 24.10.Eq, 25.40.Lw, 25.80.Nv

I. INTRODUCTION

The K^--proton interaction is a strong multichannel process [1], with the $\Lambda(1405)$ resonance just below the K^--p threshold at 1432 MeV. At low energies, the K^- can elastically scatter off the proton, charge exchange to $\overline{K^0}$-n, or scatter to $(\Sigma^+\pi^-)$, $(\Sigma^0\pi^0)$, $(\Sigma^-\pi^+)$, or $(\Lambda\pi^0)$ final states. The electromagnetic radiative capture processes $K^-p \to \Lambda\gamma$ $(\Sigma^0\gamma)$ are also possible [2]. The amplitudes of these latter reactions can be related to those of the associated strangeness photoproduction, i.e., $\gamma p \to K^+\Lambda$ $(K^+\Sigma^0)$, by crossing symmetry. Much effort has been made experimentally and theoretically to understand this system. In particular, experiments to measure the branching ratios of the radiative capture reactions $K^-p \to \Lambda\gamma$ and $K^-p \to \Sigma^0\gamma$ were recently performed [3] to help clarify the details of the reaction mechanism, with a special interest in the nature of the $\Lambda(1405)$ resonance [4]. However, on one hand the result for the $\Lambda\gamma$ channel is unexpectably smaller than both the previous measured value [5] and those obtained through phenomenological models [2], and on the other hand the measured branching ratio for the $\Sigma^0\gamma$ final states comes out significantly higher than the one for the other channel, producing yet another mystery to this already complicated problem.

The most recent measurements of the threshold branching ratios with stopped kaons, done at Brookhaven [3], are

$$R_{\Lambda\gamma} = \frac{\Gamma(K^-p \to \Lambda\gamma)}{\Gamma(K^-p \to \text{all})} = 0.86 \pm 0.07 \pm 0.09 \times 10^{-3}$$

and

$$R_{\Sigma\gamma} = \frac{\Gamma(K^-p \to \Sigma^0\gamma)}{\Gamma(K^-p \to \text{all})} = 1.44 \pm 0.20 \pm 0.11 \times 10^{-3}.$$

Existing calculations [2] overestimate $R_{\Lambda\gamma}$ by a factor of 3 or 4 (except a few recent phenomenological analysis [6,7] of the kaon photoproduction processes). The pioneer calculations considered the $\Lambda(1405)$ in two different ways: as an s-channel resonance [8] or as a quasi-bound (K-$N, \Sigma\pi$) state [9–11]. In the quark-model approaches, this hyperon is considered as a pure q^3 state [12,13], a quasi-bound $\overline{K}N$ state [14,15], or still as a hybrid (q^3+$q^4\overline{q}\cdots$) state [16–18]. A number of potential model fits to the scattering data incorporate the $\Lambda(1405)$ as a quasibound (K-$N, \Sigma\pi$) resonance [19–21]. It would be interesting to see if the radiative capture channels can also be understood within a single model, especially since the radiative capture data were taken to help distinguish between these two possibilities.

The diversified nature of the low energy data challenges theoretical models. Even if the analysis is restricted to the hadronic sector, difficulties arise when trying to understand the K^-p *1s* atomic-level shift. The sign of the K^-p scattering length extracted from this experiment is opposite to that determined from K matrix and potential model fits to the other hadronic data. This conflict poses interesting questions which are discussed in Refs. [19,20,22]. Only one potential, Ref. [20], has been published which is compatible with all the low energy hadronic data. We will examine the initial-state interactions for the radiative capture branching ratio for this potential.

Calculations which focus on the radiative capture branching ratios usually do not include the initial-state interactions. Only one group [15], which uses the cloudy bag quark model, has included these in the electromagnetic branching ratio calculation. Since the interactions are strongly coupled among the various channels, any meaningful comparison with the data needs to include channel couplings. We find here that the effect of the initial-state interactions is far from being negligible. One limitation with this latter calculation is that no comparison is made with the strong branching ratio data. The other threshold branching ratios are [23,24]

$$\gamma = \frac{\Gamma(K^-p \to \pi^+\Sigma^-)}{\Gamma(K^-p \to \pi^-\Sigma^+)} = 2.36 \pm 0.04,$$

$$R_c = \frac{\Gamma(K^-p \to \text{charged particles})}{\Gamma(K^-p \to \text{all})} = 0.664 \pm 0.011,$$

and

$$R_n = \frac{\Gamma(K^- p \to \pi^0 \Lambda)}{\Gamma(K^- p \to \text{ all neutral states})} = 0.189 \pm 0.015.$$

They put tight constraints on the threshold amplitudes and potential coupling strengths [17,20,21]. In fact, the five branching ratios are among the most precise data in the strangeness sector. However, at present there is no comprehensive analysis which includes both the hadronic and electromagnetic branching ratios of the $K^- p$ system.

The aim of this paper is to examine all the low energy data within a single model and determine if it can be understood using known coupling strengths and minimal SU(3) symmetry breaking for relevant vertices in the electromagnetic channels. In doing so, we focus on how the two radiative capture branching ratios are affected by the initial-state interactions among the different channels. In order to unravel the essential physics from the many channel system, in Sec. II we will first set up a general procedure to separate the strong (or initial-state) interactions from the electromagnetic ones. As shown in Sec. II, the initial-state hadronic interactions can be described with six complex numbers. Thus we need a model of the interaction between the strong channels to produce these six numbers. In Sec. III we examine two phenomenological potential models, each of which fits the low energy scattering data, the resonance at 1405 MeV, and the hadronic branching ratios at threshold. In one potential, the present work, the relative potential strengths between the various channels are guided by SU(3) symmetry. For this potential, the parameters are adjusted to fit all the low energy $K^- p$ data with the exception of the *1s* atomic level shift value of the $K^- p$ scattering length. The other potential is from Ref. [20], in which the scattering length is compatible with the atomic level shift data.

To clarify our discussion, we wish to underline here the nature of the fitting parameters in the potential guided by SU(3) symmetry. For the hadronic channels, the relative potential strengths are given by a value determined from SU(3) symmetry times a "breaking factor," which is equal to 1, if the the relative channel couplings are SU(3) symmetric. This SU(3) structure is motivated by chiral symmetry [14]. For a good fit to the low energy data we need to vary the relative strengths somewhat, allowing the breaking factor to deviate from 1. The final values of this factor have no obvious physical significance. The potential enables one to estimate the effects of the initial-state interactions from a potential which gives a good fit to the low energy data. In the electromagnetic channels, the radiative capture amplitudes are derived from first order "Born" photoproduction processes, which involve the meson-baryon-baryon coupling constants $g_{Kp\Lambda}$, $g_{Kp\Sigma}$, $g_{\pi\Sigma\Sigma}$, and $g_{\pi\Sigma\Lambda}$. These coupling constants are related by SU(3) symmetry to the well known πNN coupling constant. For the fit, these coupling constants are allowed to vary up to $\pm 50\%$ from their SU(3) values. Here the final values of these four parameters will have physical significance and can be compared to values derived from other analyses. Thus we will examine if the radiative capture branching ratio data can be understood using vertex coupling constants for the electromagnetic channels that are close to their expected SU(3) values when initial-state interactions are included from a hadronic interaction which fits the low energy hadronic data.

II. GENERAL FORMALISM

Consider a coupled-channel system consisting of n hadronic channels and one electromagnetic channel. We assume that the interaction between channels can be represented for each partial wave l by real potentials of the form $V_{ij}^l(\sqrt{s}, k_i, k_j)$ where $\sqrt{s}$ is the total energy and k_i is the momentum of channel i in the center-of-mass frame. We will use the notation where the indices i,j are integers for the strong channels and γ for the electromagnetic channels. We will also assume that the transition matrix element for each partial wave from channel i to channel j can be derived from a coupled-channel Lippmann-Schwinger equation:

$$T_{ij}(\sqrt{s}, k_i, k_j) = V_{ij}(\sqrt{s}, k_i, k_j) + \sum_m \int V_{im}(\sqrt{s}, k_i, q) G_m(\sqrt{s}, q) \times T_{mj}(\sqrt{s}, q, k_j) q^2 dq, \quad (1)$$

where $G_i(\sqrt{s}, q)$ is the propagator for channel i. We suppress the index l, since for our problem only the $l = 0$ partial wave is of interest. The electromagnetic coupling is weak, and to a very good approximation we can neglect the back coupling of the photon channels. Thus the T matrix for radiative capture can be written as

$$T_{i\gamma}(\sqrt{s}, k_i, k_\gamma) = V_{i\gamma}(\sqrt{s}, k_i, k_\gamma) + \sum_{m \neq \gamma} \int V_{im}(\sqrt{s}, k_i, q) G_m(\sqrt{s}, q) \times T_{m\gamma}(\sqrt{s}, q, k_\gamma) q^2 dq. \quad (2)$$

Note that in the above equation there is no integration over the photon's momentum. There is only an integration over the hadronic momentum k_i in the $V_{i\gamma}$ potential. This means that only half off-shell information is needed for the hadron-photon potential. Since $\sqrt{s}$ and k_γ are fixed in the integral, we can write $V_{i\gamma}(\sqrt{s}, q, k_\gamma)$ as

$$V_{i\gamma}(\sqrt{s}, q, k_\gamma) = \frac{V_{i\gamma}(\sqrt{s}, q, k_\gamma)}{V_{i\gamma}(\sqrt{s}, k_i, k_\gamma)} V_{i\gamma}(\sqrt{s}, k_i, k_\gamma)$$

or

$$V_{i\gamma}(\sqrt{s}, q, k_\gamma) = v_{i\gamma}(q) V_{i\gamma}(\sqrt{s}, k_i, k_\gamma). \quad (3)$$

Substituting this form for $V_{i\gamma}$ into Eq. (2) we obtain for the T matrix

$$T_{i\gamma}(\sqrt{(s)}, k_i, k_\gamma) = \sum_{m \neq \gamma} M_{im}(\sqrt{s}) V_{m\gamma}(\sqrt{s}, k_m, k_\gamma),$$

with the matrix M_{im} defined as

$$M_{im} \equiv \delta_{im} + \int V_{i,m}(\sqrt{s}, k_i, q) G_m(\sqrt{s}, q) v_{m\gamma}(q) q^2 dq + \sum_{n \neq \gamma} \int \int V_{in}(\sqrt{s}, k_i, q') G_n(\sqrt{s}, q') V_{nm}(\sqrt{s}, q', q) G_m(\sqrt{s}, q) v_{m\gamma}(q) q'^2 dq' q^2 dq + \cdots .$$

The state m is the last hadronic state before the photon is produced. Since all the on-shell momenta are determined from $\sqrt{s}$ we have

$$T_{i\gamma}(\sqrt{s}) = \sum_{m \neq \gamma} M_{im}(\sqrt{s}) V_{m\gamma}(\sqrt{s}). \quad (4)$$

This form for the transition matrix to the photon channels is very convenient, since it separates out the strong part from the electromagnetic part of the interaction. The matrix M is determined entirely from the hadronic interactions and vertices. In the absence of channel coupling M is the unit matrix. Any deviation from unity is related to the initial-state interactions. Note that *no assumptions were made on the form of the propagator or the potentials connecting the hadronic channels.* They need not be separable.

Labeling the K^--p channel as no. 5, and defining $A_m(\sqrt{s})$ as $M_{5m}(\sqrt{s})$ we can write the scattering amplitude to the photon channels as

$$F_{K^-p \to \Lambda\gamma(\Sigma^0\gamma)} = \sum A_m(\sqrt{s}) f_{m \to \Lambda\gamma(\Sigma^0\gamma)}, \quad (5)$$

where the f_m's are the amplitudes to go from the hadronic channel m to the appropriate photon channel. These amplitudes are derivable from diagrams representing the photoproduction process. The quantities A_m are unitless complex numbers, and contain all the information about the initial-state interactions for radiative capture. Generally the sum over m is restricted to states which have charged hadrons. For the K^--p process the problem is greatly simplified, since there are only three channels which have charged hadrons: $\pi^+\Sigma^-$, $\pi^-\Sigma^+$, and K^-p. To a very good approximation (see Sec. III), the A_m's are the same for both the $\Lambda\gamma$ and the $\Sigma^0\gamma$ channels. Thus three complex numbers, determined from the hadronic interactions, describe all the initial-state interactions for decays to both $\Lambda\gamma$ and $\Sigma^0\gamma$ final states.

The result of Eq. (5) is essentially Watson's theorem [25] using a particle basis. Watson's theorem, which also relates information about the strong interaction to that of the electromagnetic process, uses an isospin basis. The photoproduction amplitude is shown to have a phase equal to the hadronic phase shift for a given isospin. Equation (5) reduces to this result if there is only one strong channel. In this case, A is proportional to $e^{i\delta}$ where δ is the phase shift of the strong channel. For pion-nucleon photoproduction it is useful to use an isospin basis since the T matrix is diagonal and both the photoproduction amplitude and the hadronic phase shift can be determined from experiment. It is especially useful if one isospin dominates (i.e., the P_{33}). However, the T matrix (or potential) for the K-N, $\Sigma\pi$, $\Lambda\pi$ system is not diagonal in an isospin basis. Watson's theorem would apply to the eigenphases of the coupled K-N, $\Sigma\pi$ system for $I = 0$, and the coupled K-N, $\Sigma\pi$, $\Lambda\pi$ system for $I = 1$. Since these phases are not easily determined from experiment the results of Watson's theorem are not as useful in this case. Also, in the next section we point out that isospin breaking effects are very important at low K^--p energies. Thus, in analyzing threshold branching ratios, a particle basis is necessary. Another advantage of using Eq. (5) is that the interference of the "Born amplitudes" f due to the initial-state interactions of the hadrons is made transparent.

III. RESULTS AND DISCUSSION

A. The potentials for the strong channels

The two parts in determining the photoproduction rates in Eq. (4) are the A_m, which are determined from the strong part of the interaction, and the channel amplitudes $f_{m \to \Lambda\gamma(\Sigma\gamma)}$. For notation, we will label the channels 1–8 as $\pi^+\Sigma^-$, $\pi^0\Sigma^0$, $\pi^-\Sigma^+$, $\pi^0\Lambda$, K^-p, $\overline{K^0}n$, $\Lambda\gamma$, and $\Sigma^0\gamma$, respectively. We begin by discussing the determination of the A_m. These were obtained by using a separable potential and fitting to the available low energy data on the strong channels. We took $v_{i\gamma}$ in Eq. (3) to be equal to v_i in Eq. (6) below. Two different separable potentials were used: one guided by SU(3) symmetry for the relative channel couplings which fits all the low energy data except the *1s* atomic-level shift, and one from Ref. [20] which fits all the low energy data including the sign of the scattering length from the *1s* atomic-level shift. Values for the A_m at the K^-p threshold for each fit are listed in Table I.

Following Ref. [21] the separable potentials for the strong channels are taken to be of the form

$$V_{ij}^I(k, k') = \frac{g^2}{4\pi} C_{ij}^I b_{ij}^I v_i(k) v_j(k'), \quad (6)$$

TABLE I. The A_i values from Eq. (5) for two different strong potentials. The potential with approximate SU(3) symmetry fits all low energy hadronic data except the *1s* K^-p atomic level shift. The potential of Ref. [20] fits the atomic level shift as well.

A_i	Potential with approximate SU(3) symmetry	Potential of Tanaka and Suzuki [22]
A_1	(1.20, 0.52)	(1.49, -0.28)
A_2	(-1.02, -0.14)	(-1.10, 0.52)
A_3	(0.83, -0.23)	(0.71, -0.75)
A_4	(-0.16, -0.34)	(-0.30, -0.39)
A_5	(-0.15, 1.06)	(2.01, 2.55)
A_6	(1.18, -0.41)	(2.08, -1.12)

TABLE II. The "best fit" values of $C_{ij}^I(b_{ij}^I)$ for the potential of Eq. (6).

$C_{ij}^{I=0}$	$\Sigma\pi$	KN	
$\Sigma\pi$	-2 (0.50)	$-\frac{\sqrt{6}}{4}$ (1.29)	
KN	$-\frac{\sqrt{6}}{4}$ (1.29)	$-\frac{3}{2}$ (1.43)	
$C_{ij}^{I=1}$	$\Sigma\pi$	$\Lambda\pi$	KN
$\Sigma\pi$	-1 (0.50)	0	$-\frac{1}{2}$ (1.37)
$\Lambda\pi$	0	0	$\frac{\sqrt{6}}{4}$
KN	$-\frac{1}{2}$ (1.37)	$\frac{\sqrt{6}}{4}$	$-\frac{1}{2}$ (0.50)
$\alpha_{\Sigma_1} = 974$	$\alpha_{\Lambda\pi} = 886$	$\alpha_{KN} = 445$	$g^2 = 1.19$ fm^2

where the C_{ij}^I are determined from SU(3) symmetry. The b_{ij}^I are "breaking parameters" which are allowed to vary slightly from unity. The $v_i(k)$ are form factors, taken for this analysis to be equal to $\alpha_i^2/(\alpha_i^2 + k^2)$, and g is an overall strength constant. These potentials are used in a coupled-channel Lippmann-Schwinger equation with a nonrelativistic propagator to solve for the cross sections to the various channels. The data used in the fit are from Refs. [26–30]. The resonance at an energy of 1405 MeV was also fitted. As discussed in Ref. [21] it was not possible to fit all the low energy data using potentials that had $b_{ij}^I = 1$ for all i and j. To get an acceptable fit without including the radiative capture data, it is necessary to vary the b_{ij}^I by at least $\pm 15\%$ from unity. To get a very good fit to all the data and determine the range of the A_m, we let the b_{ij}^I vary from 0.5 to 1.5. In Table II we list the values we used for the $I = 0$ and $I = 1$ potentials for our "best fit." This "best fit" also included the radiative capture data, and is discussed in the next section. The elements are listed as a product of the C_{ij}^I values from SU(3) times b_{ij}^I which was allowed to vary from 0.5 to 1.5. Also listed are the values for α_i in MeV/c and the overall strength g^2 from Eq. (6). We note that for this fit the $\Lambda(1405)$ is produced as a K-$N(\Sigma\pi)$ bound state resonance [21] (see Fig. 4).

The A_i are a measure of how much the initial-state interactions enhance the single scattering amplitude. Not all the A_i are needed in the K^-p radiative decay calculation, since only channels which have charged particles contribute. Thus only A_1, A_3, and A_5 enter the calculation. Also due to isospin symmetry in the $\Sigma\pi$ sector A_1, A_2, and A_3 must satisfy the relation $A_1 + A_3 = -2A_2$. In the absence of initial-state interactions, $A_1 = A_3 = 0$ and $A_5 = 1$. As can be seen in Table I, the magnitudes of A_1, A_3, and A_5 are between 0.8 and 1.3. Since $F_{K^-p\to\Lambda\gamma} = A_1 f_{\Sigma^-\pi^+\to\Lambda\gamma} + A_3 f_{\Sigma^+\pi^-\to\Lambda\gamma} + A_5 f_{K^-p\to\Lambda\gamma}$, cancellations among the various amplitudes can make the radiative capture probability very sensitive to the initial-state interactions. Unfortunately, the A_i cannot be directly determined experimentally, and will have some model dependencies. We tried to estimate the model dependency for the potential of Eq. (6) by allowing the b_{ij}^I to vary different amounts between 0.5 and 1.5 and see how much the A_i changed. For acceptable fits to the data, excluding the atomic *1s* level shift, the A_i varied only $\pm 20\%$ in magnitude.

An important aspect of the problem is to include the appropriate isospin breaking effects due to the mass differences of the particles. This was done as described in Ref. [21] by using the correct relativistic momenta and reduced energies in the propagator. The effects are very important in calculating the threshold branching ratios, since the masses of $\overline{K^0}$-n are 7 MeV greater than the masses of K^-p. As shown in Ref. [31], the Coulomb po-

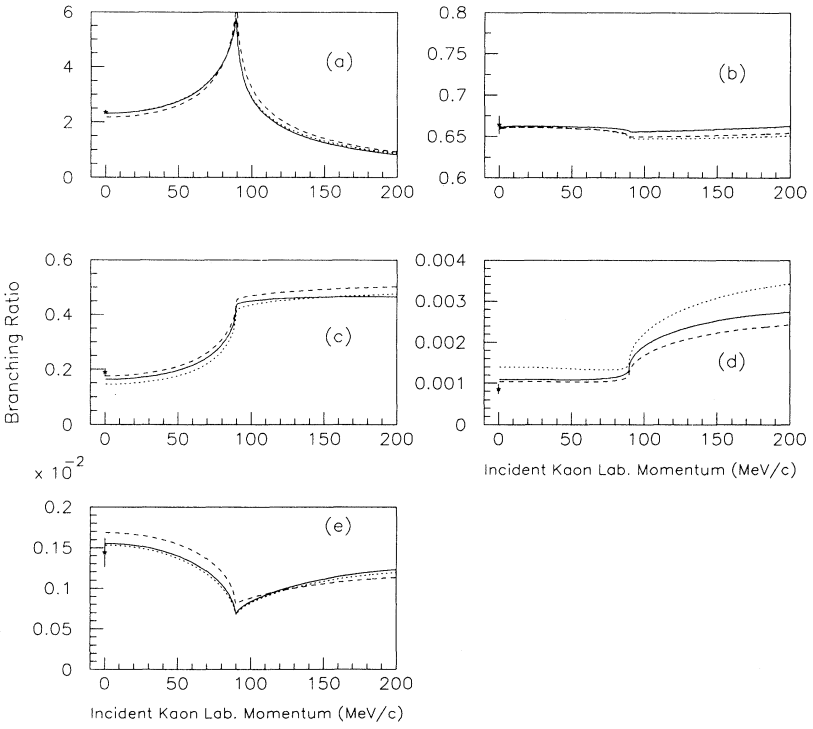

FIG. 1. The five branching ratios, defined in the text, are plotted as a function of K^- laboratory momentum: (a) branching ratio γ, (b) R_c, (c) R_n, (d) $R_{\Lambda\gamma}$, and (e) $R_{\Sigma\gamma}$. The three curves correspond to different amounts of SU(3) breaking as listed in Table III. The solid curve corresponds to our "best fit" parameters: the vertex couplings of Table V below and the strong couplings of Table II. This corresponds to the first line in Table III. The dotted curve is for $\pm 40\%$ variation in all the parameters, the third line in Table III. The dashed curve is for $\pm 30\%$ variation in all the parameters, the last line in Table III. The data points at threshold [3,19,20] with error bars are also shown. The $\overline{K^0}$-n threshold is at 89.4 MeV/c.

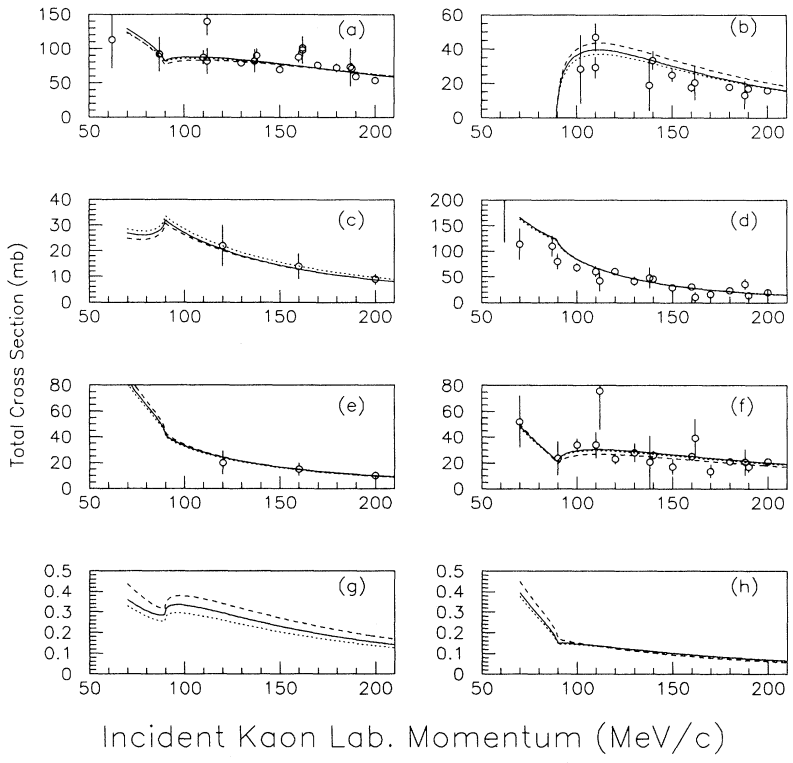

FIG. 2. Cross sections are compared with the experimental data for the six strong channels and the two electromagnetic channels: (a) K^-p elastic scattering, (b) $K^-p \to \overline{K^0}n$, (c) $K^-p \to \pi^0\Lambda$, (d) $K^-p \to \pi^+\Sigma^-$, (e) $K^-p \to \pi^0\Sigma^0$, (f) $K^-p \to \pi^-\Sigma^+$, (g) $K^-p \to \Lambda\gamma$, and (h) $K^-p \to \Sigma^0\gamma$. The three curves for each cross section correspond to different amounts of SU(3) breaking as in Fig. 1.

tential can be neglected when calculating the branching ratios. In Fig. 1 we plot the branching ratios as a function of kaon laboratory momentum $P_{\rm lab}$. The three different curves for each ratio correspond to different types of SU(3) breaking to be discussed later. Note that the energy dependence is particularly strong for branching ratios γ, R_n, $R_{\Lambda\gamma}$, and $R_{\Sigma\gamma}$.

For γ, which is the ratio of $\Sigma^-\pi^+$ production to $\Sigma^+\pi^-$ the energy dependence is easy to understand. For a model such as the one presented here which does not include the $\Lambda(1405)$ as an s-channel resonance, the reaction $K^-p \to \pi^+\Sigma^-$ cannot occur in a single step. This is a double charge exchange reaction, and needs to undergo two single charge exchange steps with the middle one being neutral. From the total cross-section data (See Fig. 2), the most important neutral channel in low energy K^-p scattering comes out to be $\overline{K^0}n$. This causes the ratio γ to have a strong energy dependence near the $\overline{K^0}n$ threshold. Since the $\overline{K^0}n$ channel is also important in $\Lambda\pi^0$ production, the ratio R_n also varies rapidly with energy near threshold. Thus for an accurate comparison with the data one needs to use a particle basis in calculating the photoproduction branching ratios at threshold. We note that, if an s-channel resonance was the dominating process in the $\Sigma\pi$ reaction, then the ratio γ would not have as rapid an energy dependence near the $\overline{K}^0n$ threshold. It is also interesting that $\Gamma(K^-p \to \Lambda\gamma)$ is substantially less than $\Gamma(K^-p \to \Sigma^0\gamma)$ at energies below the $\overline{K^0}n$ threshold and greater at energies above. Experimental data of these branching ratios near the K^-p threshold would help clarify the nature of the $\Lambda(1405)$.

B. The electromagnetic channels

We now turn our attention to the most important part of the calculation, the amplitudes for the $\Lambda\gamma$ and $\Sigma^0\gamma$ channels. As discussed previously, only the amplitudes for the three charged channels will contribute to the radiative capture amplitude in Eq. (5): $K^-p \to \Lambda\gamma(\Sigma^0\gamma)$, $\Sigma^\pm\pi^\mp \to \Lambda\gamma(\Sigma^0\gamma)$. Here we will use the amplitudes obtained from the diagrams shown in Fig. 3. These diagrams are the leading order contributions to photoproduction [32]. We include the most important amplitudes which are the "extended Born terms," including the Λ and the Σ^0 exchange terms, and the vector meson exchange terms (K^*, ρ). The expressions for these terms and their relative importance are given in the Appendix.

There are four coupling constants which enter in the photoproduction amplitudes: $g_{KN\Lambda}$, $g_{KN\Sigma}$, $g_{\pi\Sigma\Sigma}$, and $g_{\pi\Sigma\Lambda}$. Since there are only two branching ratios to fit, we need to limit the method of our search. We investigated three cases: (a) assume exact SU(3) symmetry for the coupling constants with $g_{\pi NN} = 13.4$ and vary the F-D mixing ratio α to best fit the data, (b) assume $\alpha = 0.644$, $g_{\pi NN} = 13.4$ and vary the coupling constants slightly from their SU(3) values for a best fit, and (c) use the A_m from the potential of Ref. [20] and SU(3) symmetry for the coupling constants to see if a fit of the radiative decay branching ratios is possible. For the search, we weighted each data point equally, and thus the two radiative capture branching ratios did not have a great effect on the hadronic parameters.

In the first case, we assumed exact SU(3) symmetry

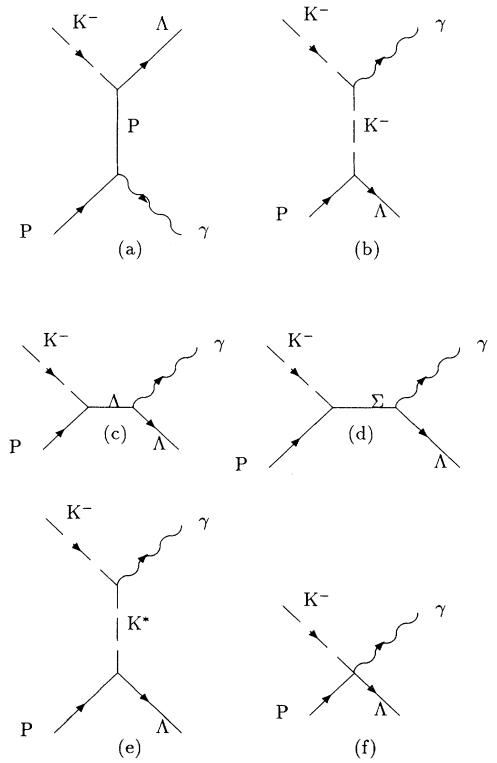

FIG. 3. The main diagrams which contribute to the radiative capture amplitude for $K^-p \to \Lambda\gamma$: (a), (b), (c), and (f) are the "Born" terms, (d) the Σ or cross term, and (e) the vector meson K^* exchange term. The $K^-p \to \Sigma^0\gamma$ reaction and the $\Sigma\pi$ reactions $\pi^\pm\Sigma^\mp \to \Lambda\gamma(\Sigma^0\gamma)$ will have similar terms.

with $g_{\pi NN} = 13.4$ and varied the F-D mixing ratio α for a best fit to the data. We found an acceptable fit with a χ^2 per data point of 2.47 for $\alpha = 1.0$. The branching ratios for this fit are $\gamma = 2.25$, $R_c = 0.66$, and $R_n = 0.17$ for the strong channels, and $R_{\Lambda\gamma} = 1.22 \times 10^{-3}$ and $R_{\Sigma\gamma} = 1.47 \times 10^{-3}$ for the electromagnetic channels. Although this is not the accepted value for α, it is remarkable to get a fit with only one adjustable variable.

In the next case, we fix α to be 0.644. The search is done using MINUIT code [33] on 13 parameters: the three ranges for the strong channels and the six breaking factors for the strong channels b^I_{ij}, $g_{Kp\Lambda}$, $g_{Kp\Sigma}$, $g_{\pi\Sigma\Sigma}$, and $g_{\pi\Sigma\Lambda}$. We allowed the b^I_{ij} to vary $\pm 50\%$, $\pm 40\%$, and $\pm 30\%$ from unity while the four coupling constants $g_{Kp\Lambda}$, $g_{Kp\Sigma}$, $g_{\pi\Sigma\Sigma}$, and $g_{\pi\Sigma\Lambda}$ varied by $\pm 50\%$, $\pm 40\%$, and $\pm 30\%$ from their SU(3) values, respectively. The range parameters α were allowed to vary from 200 to 1000 MeV/c. The results for the branching ratios and the reduced χ^2 are listed in Table III. The first column lists the percentage that the parameters, except $g_{Kp\Lambda}$, were allowed to vary from their SU(3) values (or in the case of the b^I_{ij}'s from unity). The second column lists the percentage that $g_{Kp\Lambda}$ was allowed to vary from its SU(3) value of -13.2. We also tried to find a satisfactory fit in which $g_{Kp\Lambda}$ was as close to -13.2 as possible. A fit was found in which $g_{Kp\Lambda}$ was varied only $\pm 20\%$, while the other parameters were allowed to vary $\pm 50\%$. The first row of Table III shows these results. We call this our "best fit" since the most well determined coupling constants, $g_{KN\Lambda}$ and $g_{KN\Sigma}$, are close to their SU(3) values, with $g_{KN\Sigma}$ only 50% high. Our best fit values for the coupling constants are $g_{KN\Lambda} = -10.6$, $g_{KN\Sigma} = 5.8$, $g_{\pi\Sigma\Sigma} = -7.2$, and $g_{\pi\Sigma\Lambda} = -5.0$. Notice that our values for the two first coupling constants are in agreement with those obtained from strangeness photoproduction [7,34] and hadronic sector [35,36] analyses. The electromagnetic branching ratios change drastically if the initial-state interactions are excluded from the calculation. We obtain $R_{\Lambda\gamma} = 0.56 \times 10^{-3}$ and $R_{\Sigma\gamma} = 0.12 \times 10^{-3}$ without the initial-state interactions. The two branching ratios are hence decreased by roughly a factor of 2 and more than one order of magnitude, respectively, by switching off the initial-state interactions.

Graphs of the different fits for the five branching ratios and total cross sections as a function of kaon laboratory momentum are shown in Figs. 1 and 2, respectively. In Fig. 4 we plot the $\Sigma\pi$ spectrum normalized to the data of Hemingway [37]. As in Ref. [14], we plot $k^\pi_{\text{c.m.}}|T_{\Sigma\pi\to\Sigma\pi}|^2$, where $T_{\Sigma\pi\to\Sigma\pi}$ is the T matrix in the $I = 0$ sector for $\Sigma\pi \to \Sigma\pi$ scattering. In each figure, the solid line corresponds to the "best fit" parameters, the dotted line to $\pm 40\%$ SU(3) breaking for all the parameters, and the dashed line to $\pm 30\%$ breaking for all the parameters. In each case the $\Lambda(1405)$ is produced as a bound state resonance as in Ref. [21].

The K^-p scattering length obtained from our best fit is $(-0.63 + 0.76i)$ fm. This compares closely with the value from Ref. [32] of $(-0.66 + 0.64i)$ fm. These values, however, have the opposite sign for the real part from that extracted from the *1s* K^-p atomic-level shift data [38]. Since the atomic-level shift data are still puzzling [39], we did not try to fit them in our search. This discrepancy has been discussed in detail in Ref. [20] with some interesting results. Hence we used the A_m obtained from the potential of Ref. [20] which fitted all the hadronic

TABLE III. Branching ratios and χ^2 per data point for different amounts of SU(3) breaking. Column 2 lists the variation in the coupling constant $g_{Kp\Lambda}$. Column 1 lists the variation in the other parameters.

All except $g_{Kp\Lambda}$	$g_{Kp\Lambda}$	χ^2/N	γ	R_c	R_n	$R_{\Lambda\gamma} \times 10^3$	$R_{\Sigma\gamma} \times 10^3$
$\pm 50\%$	$\pm 20\%$	1.76	2.31	0.661	0.164	1.09	1.55
$\pm 50\%$	$\pm 50\%$	1.21	2.35	0.659	0.194	0.89	1.46
$\pm 40\%$	$\pm 40\%$	1.54	2.32	0.659	0.179	1.04	1.53
$\pm 30\%$	$\pm 30\%$	2.94	2.20	0.652	0.174	1.31	1.65
Experiment			2.36 ± 0.04	0.664 ± 0.011	0.189 ± 0.015	0.86 ± 0.07	1.44 ± 0.20

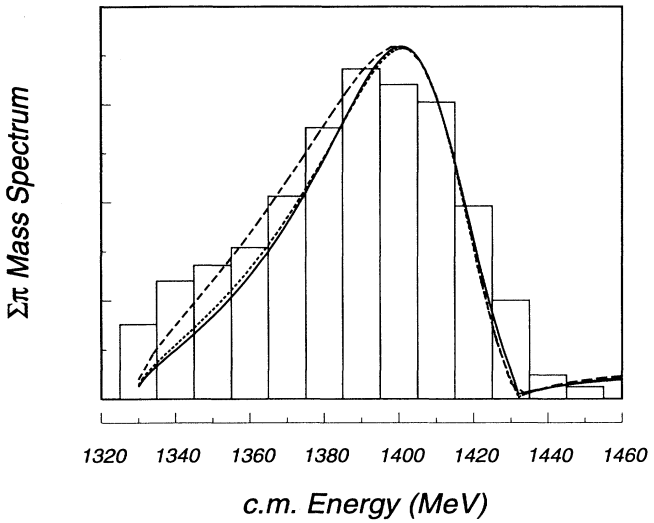

FIG. 4. The $\Sigma\pi$ mass spectrum normalized to the data of Ref. [37] is plotted as a function of the $\Sigma\pi$ center-of-mass energy. The three curves correspond to different amounts of SU(3) breaking as in Fig. 1.

low energy data and has the same sign for the scattering length as the atomic-level shift data. We were able to reproduce their results using their nonrelativistic potentials. From Table I we see that A_1 and A_3 do not differ too much from those obtained with the "SU(3) guided" potential. However, A_5 is much different in magnitude and its real part has the opposite sign. Perhaps this is because the atomic *1s* shift and hence the scattering length has the opposite sign. For the potential of [20] the resulting radiative capture branching ratios using coupling constants from SU(3) symmetry are $R_{\Lambda\gamma} = 17.5 \times 10^{-3}$ and $R_{\Sigma\gamma} = 3.29 \times 10^{-3}$, which are far from the experimental values. For satisfactory agreement with the radiative capture branching ratios, the coupling constants would have to deviate from their SU(3) values by an unreasonable amount. The reason for the bad agreement is that A_5 is very large and its real part is positive. In order to obtain a small value for $\Lambda\gamma$ production, the amplitudes have to cancel in Eq. (5). Since the relative signs of the $f_{m\to\Lambda\gamma(\Sigma^0\gamma)}$ are fixed by SU(3) symmetry, the $A_m(\sqrt{s})$ have to have appropriate relative phases to cause this cancellation. The A_m from the potential guided by SU(3) symmetry have this feature.

IV. CONCLUSIONS

We have done a comprehensive analysis of all the low energy data, except the *1s* atomic-level shift, on the K^-p system. To facilitate the analysis, we derived an expression for the radiative capture cross section which separates out the strong interaction from the electromagnetic ones. The initial-state interactions can be described by six complex amplitudes A_m, with only three of them relevant to the radiative capture process. For the strong part of the interaction we chose a separable potential whose relative potential strengths were guided by SU(3) symmetry. This potential is phenomenological and serves to produce appropriate A_m from the low energy scattering and resonance data. The radiative capture amplitudes are derived from first order "Born" photoproduction processes, and are determined from meson-baryon-baryon coupling constants, whose values are related by SU(3) symmetry to the well known πNN coupling constant.

We found a number of good fits in which the coupling constants were close to their expected SU(3) values. For these fits, the relative coupling strengths in the strong channels were guided by $SU(3)$ symmetry. In all of the fits, the $\Lambda(1405)$ is produced as a bound K-$N(\Sigma\pi)$ resonance, and the initial-state interactions were very important for the radiative capture branching ratios. The ratio $R_{\Lambda\gamma}$ varies roughly by a factor of 2, and the ratio $R_{\Sigma\gamma}$ by more than a factor of 10 due to the initial-state interactions.

Results presented in this paper, reproduce well enough the existing strong and electromagnetic data from threshold up to $P_K^{\rm lab} \approx 200$ MeV/c. Our predictions, specially for the branching ratios, show clearly the need for more experimental investigations; one of the main motivations being to clarify the nature of the $\Lambda(1405)$ resonance. Such measurements are planned at DAΦNE [40] using the tagged low energy kaon beam and may also be achieved at Brookhaven and KEK.

ACKNOWLEDGMENTS

We would like to thank J. C. David, C. Fayard, G. H. Lamot, Andreas Steiner, and Wolfram Weise for many helpful discussions and suggestions regarding this work. We are grateful to the Institute for Nuclear Theory (Seattle) for a stimulating and pleasant stay, where the idea of this collaboration emerged. One of us (P.S.) would like to thank the Centre d'Etudes de Saclay for the hospitality extended to him.

APPENDIX

In this Appendix we will summarize the contributions to the photoproduction amplitudes shown in Fig. 3. Here we will write the expressions for the $K^-p \to \Lambda\gamma$ amplitude. The amplitudes for the $K^-p \to \Sigma^0\gamma$, $\Sigma^\pm\pi^\mp \to \Lambda\gamma$, and $\Sigma^\pm\pi^\mp \to \Sigma^0\gamma$ processes will be the same with appropriate masses and coupling constants.

To lowest order the amplitude for the $K^-p \to \Lambda\gamma$ reaction f is the sum of three amplitudes,

$$f_{K^-p\to\Lambda\gamma} = F_{\rm Born} + F_\Sigma + F_{K^*},$$

which correspond to the the Born, the Σ^0, and the K^* diagrams shown in Fig. 3.

The Born amplitude is derived in Ref. [32] and is given by

TABLE IV. Values of the coupling constants which were held constant.

$\kappa_p = 1.793$	$g^V_{K^*p\Lambda} = -4.5$
$\kappa_\Lambda = -0.613$	$g^T_{K^*p\Lambda} = -16.6$
$\kappa_{\Sigma\Lambda} = 1.6$	$g^V_{K^*p\Sigma} = -2.6$
$\kappa_{K^*K} = 1.58$	$g^T_{K^*p\Sigma} = 3.2$
$\kappa_{\rho\pi} = 1.41$	$g^V_{\rho\Sigma\Lambda} = 0$
$\kappa_{\Sigma^-} = -2.157$	$g^T_{\rho\Sigma\Lambda} = 11.1$
$\kappa_{\Sigma^+} = 1.42$	$g^V_{\rho\Sigma\Sigma} = -5.2$
$\kappa_{\Sigma^0} = 0.619$	$g^T_{\rho\Sigma\Sigma} = -12.8$

$$F_{\rm Born} = -\sqrt{\frac{E_\Lambda + m_\Lambda}{2m_\Lambda}}\frac{g_{Kp\Lambda}e}{2m_p} \times \left(1 + \frac{k_\gamma}{E_\Lambda + m_\Lambda}(1 + \kappa_p + \kappa_\Lambda)\right),$$

at the K^-p threshold. The Σ term is also derived in Ref. [32] and is given by

$$F_\Sigma = -\sqrt{\frac{E_\Lambda + m_\Lambda}{2m_\Lambda}}\frac{g_{Kp\Sigma}e}{2m_p}\kappa_{\Sigma\Lambda}\frac{\sqrt{s} - m_\Lambda}{\sqrt{s} + m_\Sigma}.$$

In a similar manner, the K^* exchange term can be evaluated. In this case, there is a vector and a tensor piece. We obtain for the amplitude

$$F_{K^*} = -\sqrt{\frac{E_\Lambda + m_\Lambda}{2m_\Lambda}}\left[\frac{g^V_{K^*p\Lambda}e}{2m_p}\frac{\kappa_{K^*K}k_\gamma^2(\sqrt{s} - m_p)}{(t - m^2_{K^*})(E_\Lambda + m_\Lambda)} + \frac{g^T_{K^*p\Lambda}e}{2m_p}\frac{\kappa_{K^*K}k_\gamma^2(\sqrt{s} - m_p)}{(t - m^2_{K^*})2m_p}\left(\frac{m_\Lambda + m_p}{m_\Lambda + E_\Lambda}\right)\right].$$

In the absence of initial-state interactions, the differential cross section is given by

$$\frac{d\sigma}{d\Omega} = \frac{(E_\Lambda + m_\Lambda)(E_p + m_p)}{64\pi^2 s}\frac{P_\gamma}{P_K}|f_{K^-p\to\Lambda\gamma}|^2.$$

The first part of $F_{\rm Born}$ has the largest magnitude. The other pieces are reduced by kinematical factors, with F_{K^*} giving the smallest contribution. The K^* exchange makes up about 2% of the amplitude. Thus the uncertainty in the vector and tensor coupling constants is not so important, and we fixed them to be the SU(3) values. Also, since the calculation is not particularly sensitive to the values of the electromagnetic couplings, we fixed them at their accepted values. Values for the constants which were held fixed during the search are listed in Table IV.

TABLE V. "Best fit" values of the coupling constants for the electromagnetic amplitudes.

$g_{Kp\Lambda} = -10.6$	$g_{Kp\Sigma} = 5.8$
$g_{\pi\Sigma\Sigma} = -7.2$	$g_{\pi\Sigma\Lambda} = -5.0$

The search was done on the more important coupling constants, $g_{Kp\Lambda}$, $g_{Kp\Sigma}$, $g_{\pi\Sigma\Sigma}$, and $g_{\pi\Sigma\Lambda}$. At the K^-p threshold, using the coupling constants of Table III, the radiative capture amplitudes are

$$f_{K^-p\to\Lambda\gamma} = \frac{e}{2m_p}[-g_{Kp\Lambda}(1.28) - g_{Kp\Sigma}(0.2) - 0.75],$$

$$f_{K^-p\to\Sigma^0\gamma} = \frac{e}{2m_p}[-g_{Kp\Sigma}(1.32) - g_{Kp\Lambda}(0.15) + 0.02],$$

$$f_{\pi^+\Sigma^-\to\Lambda\gamma} = \frac{e}{2m_\Sigma}[-g_{\pi\Sigma\Lambda}(0.835) + g_{\pi\Sigma\Sigma}(0.19) + 0.21],$$

$$f_{\pi^+\Sigma^-\to\Sigma^0\gamma} = \frac{e}{2m_\Sigma}[-g_{\pi\Sigma\Sigma}(0.95) + g_{\pi\Sigma\Lambda}(0.153) + 0.19],$$

$$f_{\pi^-\Sigma^+\to\Lambda\gamma} = \frac{e}{2m_\Sigma}[g_{\pi\Sigma\Lambda}(1.16) - g_{\pi\Sigma\Sigma}(0.19) - 0.21],$$

$$f_{\pi^-\Sigma^+\to\Sigma^0\gamma} = \frac{e}{2m_\Sigma}[-g_{\pi\Sigma\Sigma}(1.28) + g_{\pi\Sigma\Lambda}(0.153) + 0.19],$$

where the three terms in square brackets correspond to the three amplitudes described above. The above equations show the relative importance of the different contributions to radiative capture at the K^-p threshold. The best fit values for these coupling constants are summarized in Table V.

[1] See, e.g., A.J.G. Hey and R.L. Kelly, Phys. Rep. **96**, 71 (1983).

[2] See, e.g., J. Lowe, Nuovo Cimento **A102**, 167 (1989), and references therein.

[3] D.A. Whitehouse *et al.*, Phys. Rev. Lett. **63**, 1352 (1989).

[4] See, e.g., R.C. Barrett, Nuovo Cimento A **102**, 179 (1989).

[5] J. Lowe *et al.*, Nucl. Phys. **B209**, 16 (1982).

[6] R. Williams, C. Ji, and S. Cotanch, Phys. Rev. C **46**, 1617 (1992).

[7] J.C. David, C. Fayard, G.H. Lamot, F. Piron, and B. Saghai, in *Proceedings of the 8th Symposium on Polarization Phenomena in Nuclear Physics*, Bloomington, 1994, edited by S. Vigdor *et al.* (AIP, New York, in press); J.C. David, Ph.D. thesis, Univerity of Lyon, 1994 (in French).

[8] T.A. DeGrand and L. Jaffe, Ann. Phys. (N.Y.) **100**, 425 (1976); T.A. DeGrand, *ibid.* **101**, 496 (1976).

[9] G. Rajasekaran, Phys. Rev. D **5**, 610 (1972).

[10] R.H. Dalitz and S.F. Tuan, Ann. Phys. (N.Y.) **10**, 307 (1960).

[11] R.H. Dalitz, T.-C. Wong, and G. Rajasekaran, Phys. Rev. **153**, 1617 (1967).

[12] M. Jones, R.H. Dalitz, and R.R. Horgan, Nucl. Phys. **B129**, 45 (1977).

[13] J.D. Darewych, R. Koniuk, and N. Isgur, Phys. Rev. D **32**, 1765 (1985).
[14] E.A. Veit, B.K. Jennings, A.W. Thomas, and R.C. Barrett, Phys. Rev. D **31**, 1033 (1985).
[15] Y.S. Zhong, A.W. Thomas, B.K. Jennings, and R.C. Barrett, Phys. Rev. D **38**, 837 (1988).
[16] E. Kaxiras, E.J. Moniz, and M. Soyeur, Phys. Rev. D **32**, 695 (1985).
[17] G. He and R.H. Landau, Phys. Rev. C **48**, 3047 (1993).
[18] M. Arima, S. Matsui, and K. Shimizu, Phys. Rev. C **49**, 2831 (1994).
[19] J. Schnick and R.H. Landau, Phys. Rev. Lett. **58**, 1719 (1987).
[20] K. Tanaka and A. Suzuki, Phys. Rev. C **45**, 2068 (1992).
[21] P.B. Siegel and W. Weise, Phys. Rev. C **38**, 2221 (1988).
[22] K.S. Kumar and Y. Nogami, Phys. Rev. D **21**, 1834 (1980).
[23] R.J. Nowak *et al.*, Nucl. Phys. **B139**, 61 (1978).
[24] D.N. Tovee *et al.*, Nucl. Phys. **B33**, 493 (1971).
[25] K.M. Watson, Phys. Rev. **95**, 228 (1954).
[26] J. Ciborowski *et al.*, J. Phys. G **8**, 13 (1982).
[27] D. Evans *et al.*, J. Phys. G **9**, 885 (1983).
[28] W.E. Humphrey and R.R. Ross, Phys. Rev. **127**, 1305 (1962).
[29] J.K. Kim, Columbia University Report No. Nevis 149, 1966.
[30] M. Sakitt *et al.*, Phys. Rev. **139**, 719 (1965).
[31] P.B. Siegel, Z. Phys. A **328**, 239 (1987).
[32] R.L. Workman and H.W. Fearing, Phys. Rev. D **37**, 3117 (1988).
[33] F. James, Proceedings of the 1972 CERN Computing and Data Processing School, Pertisan, Austria, 1972, CERN Report No. 72-21, 1972; F. James and M. Roos, "MINUIT Functional Minimization and Error Analysis," CERN Report No. D506-Minuit, 1989.
[34] R.A. Adelseck and B. Saghai, Phys. Rev. C **42**, 108 (1990).
[35] A.D. Martin, Nucl. Phys. B **179**, 33 (1981); J. Antolin, Z. Phys. C **31**, 417 (1986).
[36] M. Bozoian, J.C. van Doremalen, and H.J. Weber, Phys. Lett. B **122**, 138 (1983).
[37] R. Hemingway, Nucl. Phys. **B253**, 742 (1985).
[38] J.D. Davies *et al.*, Phys. Lett. B **83**, 55 (1979); M. Izycki *et al.*, Z. Phys. A **297**, 11 (1980); P.M. Bird, A.S. Clough, and K.R. Parker, Nucl. Phys. A **404**, 482 (1983).
[39] C.J. Batty, Nuovo Cimento **A102**, 255 (1989).
[40] See, e.g., Proceedings of the Workshop on Physics and Detectors for DAΦNE, Frascati, Italy, 1991, edited by G. Pancheri, servizio documentazione de Laboratori Nazionali di Frascati, 1991; FINUDA Collaboration, "A Detector for Nuclear Physics at DAΦNE," Frascati Report No. LNF-93/021, 1993.